Segmentation of B-mode and Elastography Images

Abhishek Tiwari
B.Tech-M.Tech Dual Degree
Dept. of Electrical Engineering
IIT Kanpur, Kanpur, India
tiwaria9034@gmail.com

Srinivas Kudavelly
Software Architect
Philips Innovation Campus
Bangalore, India
srinivas.kudavelly@philips.com

***Abstract*—Ultrasound has been an important imaging technique for detecting breast tumors. As opposed to the conventional B-mode image, the ultrasound elastography is a new technique for imaging the elasticity and applies to detect the stiffness of tissues. In this paper, we proposed a CAD system to extract the features for efficient classification of the tumor into benign and malignant. The lesion boundaries were automatically delineated using active contour methods, applied individually to both b-mode and elasto-images. Four elastographic and four b-mode features were extracted from the overlapping area of the delineated boundary for the tumor classification into benign and malignant. In our experiment, a dataset of pathologically-proven 69 images including 35 benign and 34 malignant breast lesions were used to examine the classification.**

Keywords-Breast tumor, Elastography, B-mode, Ultrasound, Computer-aided diagnosis, Segmentation

I. INTRODUCTION

Breast Cancer is the second leading cause of death of women worldwide, and more than 8% of all women will suffer this disease during their lifetime [1]. According to Sivaramakrishna et al. [2], breast cancer is most effectively traded when detected at an early stage, where imaging techniques play an important role. Many computerized schemes initially return a number of locations called "potential lesion" sites. These are the regions which computer deems suspicious and require a close examination. A lesion segmentation algorithm is them employed to extract the lesion or potential lesion from its surrounding tissues. Features can then be calculated using the segmentation information and classification can be accomplished using these features.

Until recently, the most effective modality for detecting and diagnosing breast tumor has been **mammography** [3], [4]. However, there are limitations of mammography in breast cancer detection. Low specificity of mammography results in many unnecessary (65-85%) biopsy operations [5]. The unnecessary biopsies not only increase the cost, but also make the patients suffer from emotional pressure. In addition, the ionizing radiation of mammography might be harmful for both patients and radiologists.

Ultra-Sound (US) imaging, also called sonography, is a technique in which high-frequency sound waves are bounced off tissues and internal organs. Sound waves are pressure variations forming a longitudinal wave whose echoes produce a picture called a sonogram. US imaging of breast has been primarily used to distinguish between solid tumors and fluid-filled cysts.

Elastography, is a dynamic imaging technique that uses sonographic information to provide an estimate of tissue stiffness by measuring the degree of deformation under the application of an external force. This technique is based on the principle that the soft parts of tissues deform more easily than harder parts of tissue under compression, thus allowing an objective determination of tissue consistency [8] – [10]. Since breast tissue is soft as well as compressible, and because breast cancer tissue is harder than normal breast tissue, thus leading to a difference in strain, elastography has been studies as a tool for classification of benign and malignant breast masses.

II. BACKGROUND

A. Computer-aided Diagnosis

It helps remove the inter-observer variability and to help radiologists in making accurate diagnoses. One advantage of a CAD system is that it can obtain some features, such as computational and statistical features, which cannot be obtained visually and intuitively by medical doctors. Another advantage is that CAD can minimize the operator –dependent nature inherent in ultrasound imaging [17] and make the diagnosis process more reproducible. It should be noted that research into the use of CAD is not done so with an eye towards eliminating doctors or radiologists, rather the goal is to provide doctors and radiologists a second opinion and help them to increase the diagnosis accuracy, reduce biopsy rate, and save them time and effort.

Generally, ultrasound CAD systems for breast cancer detection involve four stages, as shown in figure 1.1

1. Image preprocessing: The task of image preprocessing is to enhance the image and to reduce speckle without destroying the important features for BUS images for diagnosis.
2. Image segmentation: It divides the image into non-overlapping regions, and it separates the objects (lesions) from the background. Lesion boundaries are delineated for feature extraction.
3. Feature extraction and selection: This step is to find a feature set of breast cancer lesions that can accurately distinguish lesion/non-lesion or benign/malignant.

4. Classification: Based on the selected features, the suspicious regions can be classified into different categories, such as benign or malignant findings. Many machine learning techniques such as support vector machines (SVM), and artificial neural networks (ANN) have been studied for lesion classification.

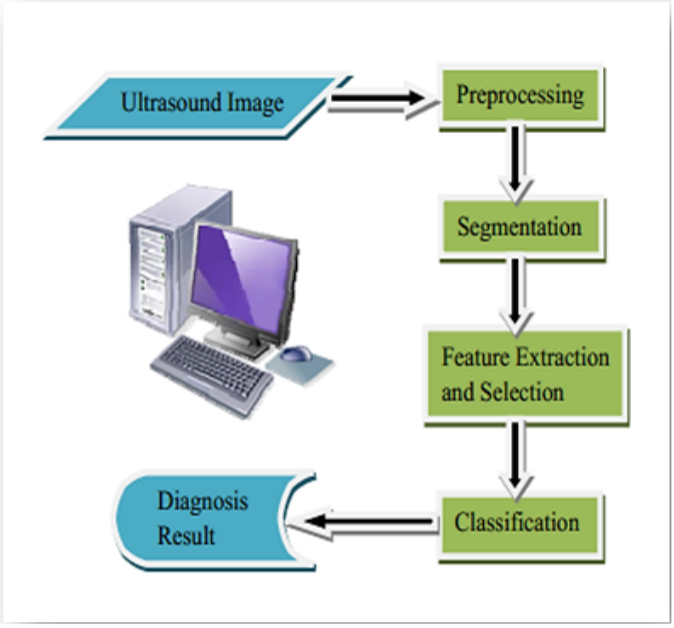

Fig. 2.1. A CAD system for breast cancer diagnosis.

B. *Challenges – US artifacts*

US images are generated by fundamental properties such as acoustic impedance and physical density. However, due to its strongly nonlinear behavior the brightness of each blob not only depends on physical properties (density and acoustic impedance) of the imaged blob, but also on the physical properties of the surrounding tissue.

Due to its process of formation, US B-mode images have some artifacts, which are described as follows:

1. **Speckle:** Speckle arises from micro scatterers located throughout the tissue, so that even in the same tissue, it appears as a granular structure superimposed in the image. Speckle is detrimental because it reduces both image contrast (the ability to see a desired structure against a background).
2. **Shadowing:** The shadowing effect occurs when the whole ultrasonic beam is attenuated by a structure within the B-mode scan range. This effect can be observed on US B-mode image as a dark shadow beyond which there is no speckle.

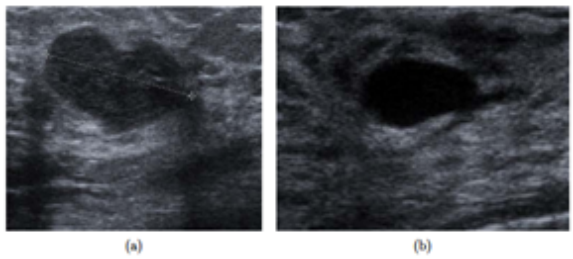

Fig. 2.2. Shadowing artifact in US image examples. (a) Presence of shadows due to attenuation of the media. (b) Cyst without shadow artifact presence.

C. *Existing methods*

Commonly used segmentation approaches are summarized in Table 2.1.

TABLE 1. SUMMARY OF SEGMENTATION METHODS FOR BUS IMAGES

Methods	Descriptions	Advantages	Drawbacks
Histogram Thresholding	Threshold value is selected to segment the image.	Simple and fast.	Works only for bimodal histograms and has no good results for BUS images.
Region growing	Region is grown from the seed point by adding similar neighboring pixels.	Simple concept. Multiple stop criteria can be chosen.	Seed point is requires; sensitive to noise.
Model based (includes active contour, level set, Markov random fields)	A model is used to formulate the lesion contour, and the model is revised based on local features such as edges, intensity gradient, texture, etc.	Robust, self-adapting in search of minimal energy.	Time consuming; pre-labeled ROI or initial contour is required; easy to get stuck in local minima states.
Machine learning	Features to separate the lesion from the background are extracted first, and a machine learning method is trained to do the classification.	Stable; different lesion characteristics can be incorporated by feature extraction.	Long training time; over-training problem; test images should come from the same platform as the training images.
Watershed (includes marker-controlled and cell-competition)	Considers image as topographic surface wherein grey level of a pixel is interpreted as its altitude. Water flows along a path to finally reach a local minimum.	It ensures closed region boundaries.	Over-segmentation problem is not completely solved.

III. PROPOSED APPROACH

In current practices, the elastography images are presented side by side with 2D US B-mode image. The user needs to manually identify the probable lesions and draw corresponding boundaries around the lesions, and then the system displays the measured area and ratio of areas of strain elastography image and US B-mode images. The main drawback is that the user (doctor or radiologist) is expected to draw the boundary across the probable lesions which are not very accurate. This manual boundary delineation makes the process subjective, and it highly depends upon the expertise of the user. Also, the lesions which are smaller in size may miss the attention of the user.

The aim of this work was to investigate the feasibility of an algorithm which will automatically detect the lesion boundary for the Elastography images.

A. Flowchart

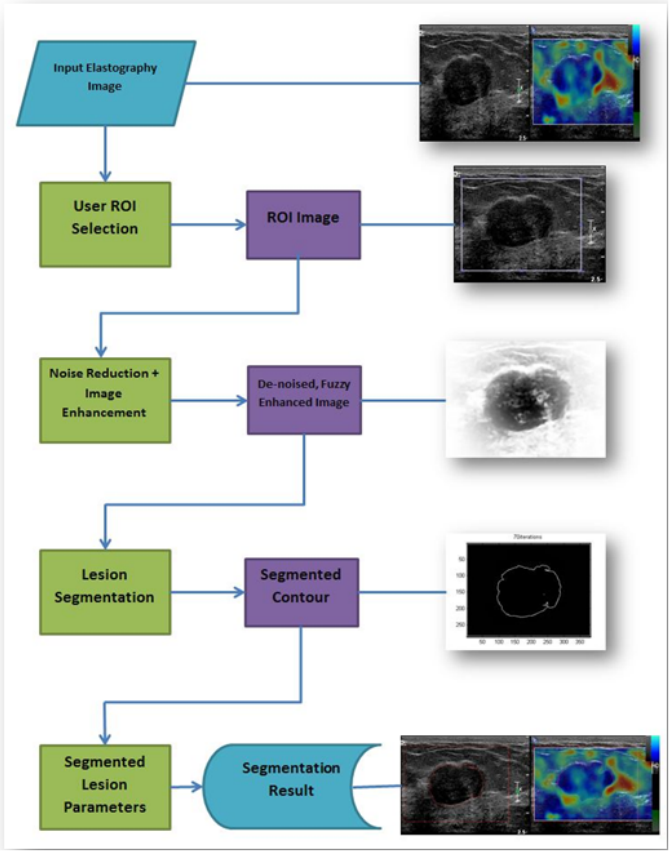

Fig. 3.1. Flowchart for implemented algorithm

B. Image Pre-processing

Image region of interest (ROI) was selected by user from either B-mode or elasto-image, depending upon which image had greater contrast between lesion and background. The selected ROI was subjected to median filtering, with filter size 7x7, in order to remove speckle noise. The selection of ROI made the process of lesion segmentation less computationally expensive, as further processing was done on the ROI image itself.

The histogram of the ROI image was equalized in order to spread out the pixel intensity histogram to make image features more distinguishable. Following step was the pixel-wise product of ROI image pixel-values with the 2D isotropic Gaussian function, having image center as Gaussian center, in order to enhance the lesion contrast, assuming lesion is centered at ROI center.

The image (selected ROI) histogram was then equalized in order to increase the contrast between lesion and the background. Next the image enhancement technique based on fuzzy logic, as described in [49], was implemented to further enhance the image. The method consists of 1) Image Normalization. 2) Fuzzification. 3) Enhancement.

1) Image Normalization: Normalization is necessary since the distribution of grey levels of breast cancer ultrasound images may vary large and the ranges of the intensities are narrow. We map the intensity levels into the range [g(min), g(max)] using the linear transformation. Here g(min) = 0, g(max) = 1.

$$g(i,j) = g(\min) + \frac{\left(g(\max) - g(\min)\right) X \left(g'(i,j) - g'(\min)\right)}{\left(g'(\max) - g'(\min)\right)} \quad (1)$$

where $[g'(\min), g'(\max)]$ are the minimum and maximum intensity levels of the original image, g'(i,j) is the grey level of pixel(i,j) before normalization.

2) Fuzzification: In fuzzy logic, the fuzzy membership function is a mapping from an element to a real value within [0,1]. In order to apply the fuzzy logic to BUS images, a suitable membership function should be found and it should map all elements in the set into [0,1].

We used the S-function as our membership function. The definition is following [50]:

$$\mu_x(i,j) = S(g,x,y,z) = \begin{cases} 0 & 0 \le g \le x \\ \frac{(g-x)^2}{(y-x)(z-x)} & x \le g \le y \\ 1 - \frac{(g-z)^2}{(z-y)(z-x)} & y \le g \le z \\ 1 & g \ge z \end{cases} \quad (2)$$

The values of $\mu_x(i,j)$ represents the brightness degrees of the pixel intensities.

The degree of ambiguity in an image X can be measured by the entropy of the fuzzy set as following:

$$H(X) = \frac{1}{M \times N} \sum_{i=1}^{M} \sum_{j=1}^{N} S_x\left(\mu_x(g_{ij})\right) \quad (3)$$

S_{x0} is the Shannon function. The formula is following:

$$S_n\left(\mu_x(g_{ij})\right) = -\mu_x(g_{ij}) log_2 \mu_x(g_{ij}) - \left(1 - \mu_x(g_{ij})\right) log_2\left(1 - \mu_x(g_{ij})\right)$$
$$i = 1,2,\ldots,M,\ j = 1,2,\ldots\ldots,N \quad (4)$$

The maximum fuzzy entropy principle: the greater value of entropy is, the more information of the system is included [51]. We will find the optimal parameters which gives the largest valued $H(X)$.

3) Enhancement: Image enhancement is one of the most important step in low-level image processing. The purpose of this step is to improve the quality of low contrast images. Therefore, the underlying principle of the enhancement is to enlarge the intensity difference between objects and the surroundings.

We use the under equation to make background and objects more distinguishable.

$$\mu_{EN(A)}(x) = \begin{cases} 2\left(\mu_A(x)\right)^2 & 0 \le \mu_A(x) \le 0.5 \\ 1 - 2\left(1 - \mu_A(x)\right)^2 & 0.5 < \mu_A(x) \le 1 \end{cases} \quad (5)$$

Then the given ultrasound image can be mapped from the intensity space domain (g_{ij}) to fuzzy domain $(\mu_x(g_{ij}))$.

Lastly in the pre-processing step, the pixel-wise product of ROI image pixel-values with the 2D isotropic Gaussian function, having image center as Gaussian center, to further make the lesion more distinguishable from background.

C. Image Segmentation

Image segmentation is a fundamental problem in image processing and computer vision. The active contour method described in [56] was used for segmentation of pre-processed image. It is implemented with a special processing named *Selective Binary and Gaussian Filtering Regularized Level Set (SBGFRLS)* method, which first selectively penalizes the level set function to be binary, and then uses a Gaussian smoothing kernel to regularize it. The B-mode images and elastography images were segmented separately for lesion boundary demarcation.

D. Feature Extraction

Lesion features were computed for segmented images for the classification of tumor as benign or malignant. The hue value in color elastography images was considered equivalent to gray-level pixel intensity in the gray elastography images. The hue component was selected as the color in the RGB elastography images contained the hardness information as shown in Fig. 3.4. In [60], features such as strain difference, strain ratio, mean strain, etc were calculated from the elasto-image while features like orientation, undularity, average gradient, intensity variance, etc were calculated for the segmented lesion on B-mode images. There was a clear demarcation between benign and malignant tumor according to these computed features.

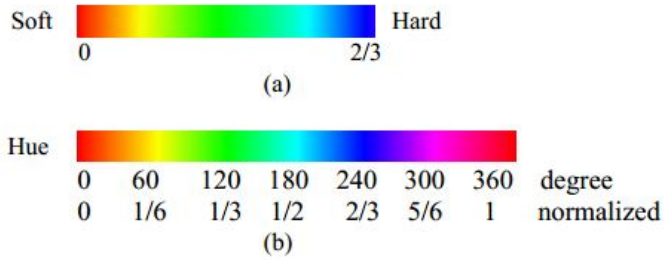

Fig. 3.4. (a) Color scale of elastography. (b) Hue scale of the HSV color space

In yet another study for tumor classification [61], segmented lesion features such as tumor mean hardness, inner mean hardness, outer mean hardness, hard rate, inner hard rate and outer hard rate were computed from color elastography images. The stepwise flowchart for the calculation of features is shown in Fig. 3.5.

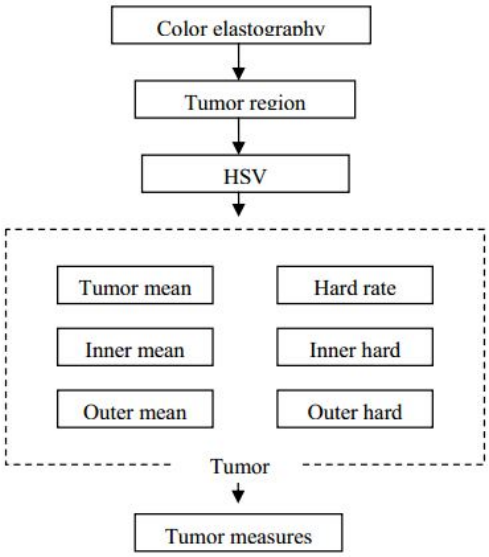

Fig. 3.5. Flowchart for elastography analysis

In our experiment, we computed the following features from the elastographic strain image:

1. Lesion mean hardness (or strain)
2. Lesion hardness variance
3. Strain ratio
4. Percentage of pixels having hardness greater than a fixed threshold (as shown in Fig. 3.6)

For B-mode image, the features computed were:

1. Gray-level pixel intensity variance
2. Average gradient
3. Gradient variance
4. Gray–level entropy

All the above features were calculated for the image area which was segmented as lesion in both B-mode and

elastography images, using the formulas same as derived in [60] & [61].

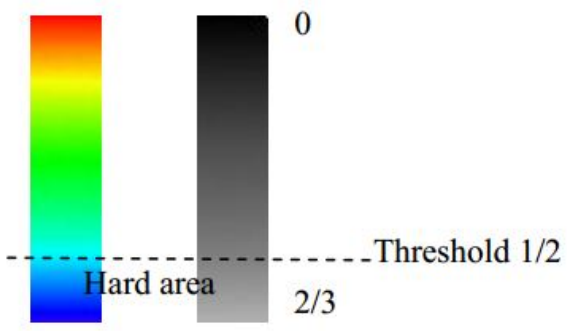

Fig. 3.6. The threshold of hard tumor

E. Results

In our experiment, a dataset of pathologically-proven 69 images including 35 benign and 34 malignant breast lesions were used for segmentation of tumors and feature extraction for tumor classification. The mean values of the four elastographic image features (mean hardness, hardness variance, strain ratio, above threshold hardness) and the four B-mode image features (pixel intensity variance, average gradient, gradient variance and gray-level entropy) were significantly different between benign and malignant tumors as tabulated in Table 2.

TABLE 2. THE MEAN AND STANDARD DEVIATION VALUES OF VARIOUS ELASTOGRAPHIC AND B-MODE FEATURES IN THE BENIGN AND MALIGNANT CASES

	Mean ± SD	
Features	Benign	Malignant
Elastographic		
mean hardness	0.522 ± 0.259	0.567 ± 0.272
hardness variance	0.057 ± 0.037	0.048 ± 0.029
strain ratio	1.204 ± 0.588	1.161 ± 0.599
above threshold hardness percentage	42.383 ± 28.450	47.007 ± 32.144
B-mode		
intensity variance	0.021 ± 0.013	0.020 ± 0.012
average gradient	0.105 ± 0.081	0.102 ± 0.076
gradient variance	0.009 ± 0.007	0.007 ± 0.005
gray-level entropy	5.603 ± 1.685	6.007 ± 1.447

The scatter plots of some of the features extracted for lesion classification are shown in Fig. 3.7 – Fig. 3.9. On the average, the points corresponding to benign and malignant tumors are distinguishable.

Fig. 3.7. Scatter plot graph of average lesion hardness (elastographic feature).

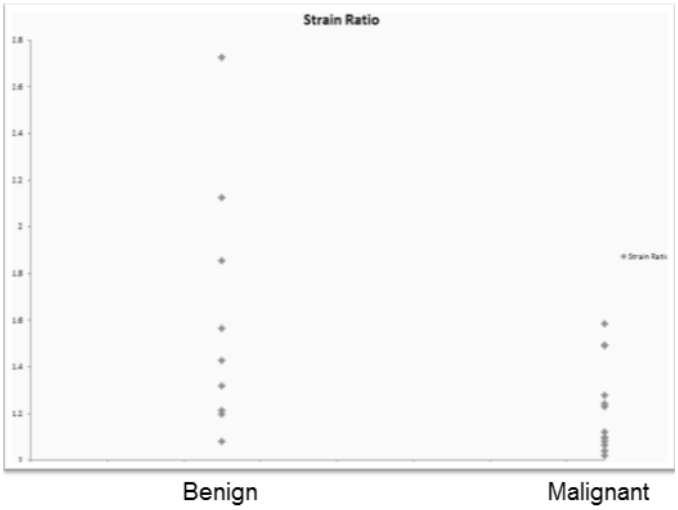

Fig. 3.8. Scatter plot graph of strain ratio (elastographic feature).

Fig. 3.10 shows the segmentation of the phantom tissue image, which is used as a standard test measure for segmentation algorithms. In a phantom, a lead ball is placed inside the tissue which corresponds to hardening of the tissue at that position. The rectangular box surrounding the segmented boundary was the region of interest (ROI), as specified by the user. The algorithm was able to clearly demarcate the boundary corresponding to the hard tissue. Another result with segmentation algorithm applied to color elastographic image has been shown in Fig. 3.11. The blue color in the elasto-image corresponds to the hard tissue, corresponding to dark lesion in the B-mode image. The dark lesion boundary and the corresponding hardness were efficiently segmented by the algorithm.

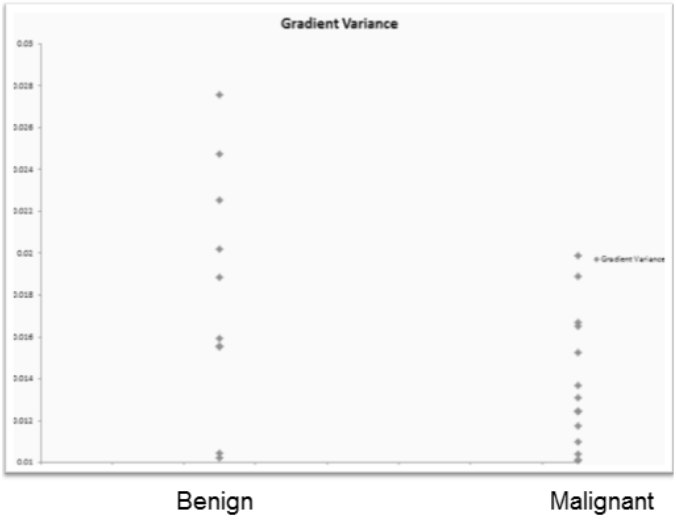

Fig. 3.9. Scatter plot graph of average gradient (b-mode feature).

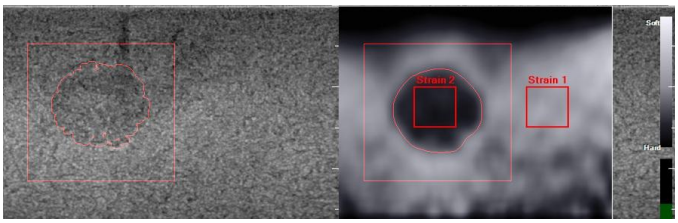

Fig. 3.10. Segmentation algorithm applied to phantom tissue.

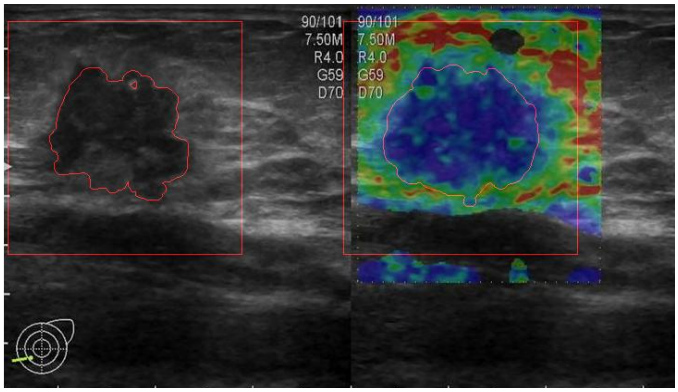

Fig. 3.11. Segmentation algorithm applied to color elastography image.

IV. DISCUSSION

Ultrasound elastography is used to measure the elasticity of the breast by the compression strain. In this paper, we aimed to propose a computer-aided diagnosis for effective distinguishing benign and malignant tumors based on elastographic information. Firstly, the elastographic images were segmented, then, four elastographic image and four b-mode image features were extracted from the algorithm delineated lesion boundary to serve the purpose of classification. Thus, the proposed CAD system considers both the elasticity information and the conventional B-mode information.

The eight features extracted can be used as an input to a neural network for efficient classification of segmented lesion boundaries in the future work. The classification performance can be further enhanced by finding the optimal feature.

REFERENCES

1. Cheng HD, Shan J, Ju W, Guo Y, and Zhang L. Automated breast cancer detection and classification using ultrasound images: A survey. *Pattern Recognition 43*, 1(2010), 299-317.
2. Radhika Sivaramakrishna, Kimerly A Powell, Michael L Lieber, William A Chilcote, and Raj Shekhar. Texture analysis of lesions in breast ultrasound images. *Computerized medical imagiing and graphics: the official journal of the Computerized Medical Imaging Society,* 26(5): 303-7, Jan 2002.
3. Cheng HD, Shi XJ, Min R, Hu LM, Cai XP, and Du HN. Approaches for automated detection and classification of masses in mammograms. *Pattern Recognition 39*, 4(2006), 646-668.
4. Cheng HD, Cai X, Chen X, Hu L, and Lou X. Computer-aided detection and classification of microcalcifications in mammograms: A survey. *Pattern Recognition 36*, 12(2003), 2967-2991.
5. Jesnek J, Lo J, and Baker J. Breast mass lesions: Computer-aided diagnosis models with mammographic and sonographic descriptors. *Radiology 244*, 2(2007), 390-398.
6. A Thomas Stavros, Cynthia l. Rapp, and Steve H. Parker. Breast ultrasound. Page 1015, Jan 2004.
7. K Taylor, C Merritt, C Piccoli, and R Schmidt. Ultrasound as a complement to mammography and breast examination to characterize breast masses. *Ultrasound in Medicine & Biology,* Jan 2002.
8. Sarvazyan AP, Rudenko OV, Swanson SD, Fowlkes JB, Emelianov SY. Shear wave elasticity imaging: a new ultrasonic technology of medical diagnostics. *Ultrasound Medicine & Biology* 1998; 24:1419-1435.
9. Cho N, Moon WK, Park JS, Cha JH, Jang M, Seong MH. Nonpalpable breast masses: evaluation by US elastography. *Korean J Radiol* 2008; 9:111-118.
10. Qiu Y, Sridhar M, Tsou JK, Lindfors KK, Insana MF. Ultrasonic viscoelasticity imaging of nonpalpable breast tumors: preliminary results. *Acad Radiol* 2008; 15:1526-1533.
11. Ophir J, Cespedes I, Ponnekanti H, Yazdi Y, Li X. Elastography: a quantitative method for imaging the elasticity of biologica tissues. *Ultrasound imaging* 1991; 13:111-134.
12. Garra BS, Cespedes EI, Ophir J. Elastography of breast lesions: initial clinical results. *Radiology*1997; 202:79-86.
13. American College of Radiology. *Breast Imaging Reporting and Data System: Ultrasound.* 4th ed. Reston, VA: American College of Radiology; 2003.
14. Hong AS, Rosen EL, Soo MS, Baker JA. BI-RADS for sonography: positive and negative predictive values of sonographic features. *AJR Am J Roentgenol* 2005; 184:1260-1265.
15. Costantini M, Belli P, Lombardi R, Franceschini G, Mule A, Bonomo L. Characterization of solid breast masses: use of sonographic Breast Imaging Reporting and Data System lexicon. *J Ultrasound Med* 2006; 25:649-659.
16. Krouskop TA, Wheeler TM, Kallel F, Garra BS, Hall T. Elastic moduli of breast and prostrate tissues under compression. *Ultrasound Imaging* 1998; 20:260-274.
17. Hwang KH, H Lee, JG Kim, Lee HJ, Om KS, Yoon M, and Choe W. Computer aided diagnosis (CAD) of breast mass on ultrasonography and scintimammography. In *Proceedings of 7th International Workshop on Enterprise Networking and Computing in Healthcare Industry*, 2005, 187-189.
18. Joo S, Moon WK, and Kim HC. Computer-aided diagnosis of solid breast nodules on ultrasound with digital image processing and artificial neural network. In *26th Annual IEEE International Conference Proceedings on Engineering in Medicine and Biology Society,* 2004, 1397-13400.
19. Chen DR, Chang RF, and Huang YL. Computer-aided diagnosis applied to US of solid breast nodules by using neural networks. *Radiology 213*, 2(1999), 407-412.

20. Madabhushi A, and Metaxas DN. Combining low-, high-level and empirical domain knowledge for automated segmentation of ultrasonic breast lesions. *IEEE Trans. On Medical Imaging 22*, 2(2003), 155-169.
21. Xiaohui H, Bruce CJ, Pislaru C, and Greenleaf JK. Segmenting high-frequency intracardiac ultrasound images of myocardium into infracted, ischemic, and normal regions. *IEEE Trans. On Medical Imaging 20*, 12(2001), 1373-1383.
22. Alwaleed Abderahman, Omer Hamid (2011). Lesion boundary detection in ultrasound breast images. *IEEE Conf. on Biomedical Engineering*, pp. 320-323.
23. Moi Hoon Yap, Eran A Edirisinghe, and Helmut E Bez. Object boundary detection in Ultrasound images. *Conference on Computer and Robot Vision 2006.*
24. A Madabhushi, and DN Metaxas. Automated boundary extraction of ultrasonic breast lesions, in *Proc. IEEE Int. Symp. Biomedical Imaging*, 2002, pp.601-604.
25. Chang RF, Wu WJ, Moon WK, and Chen DR. Automatic ultrasound segmentation and morphology based diagnosis of solid breast tumors. *Breast Cancer Research and Treatment 89*, 2(2005), 179-185.
26. Liu B, Cheng HD, Huang J, Tian J, Liu J, and Tang X. Automated segmentation of ultrasonic breast lesions using statistical texture classification and active contour based on probability distance. *Ultrasound im Medicine & Biology 35*, 8(2009), 1309-1324.
27. Sarti A, Corsi C, Mazzini E, and Lamberti C. Maximum likelihood segmentation with Rayleigh distribution of ultrasound images. *Computers on Cardiology 31* (2004), 329-332.
28. Chang RF, Wu WJ, Moon WK, Chen WM, Lee W, and Chen DR. Segmentation of breast tumor in three-dimensional ultrasound images using three-dimensional discrete active contour model. *Ultrasound in Medicine & Biology 29*, 11(2003), 1571-1581.
29. Chen DR, Chang RF, Wu WJ, Moon WK, and Wu WL. 3-D breast ultrasound segmentation using active contour model. *Ultrasound in Medicine & Biology 29*, 7(2003), 1017-1026.
30. Chang RF, Wu WJ, Tseng C, Chen DR, and Moon WK. 3-D snake for US in margin evaluation for malignant breast tumor excision using mammotome. *IEEE Trans. On Information Technology in Biomedicine 7*, 3(2003), 197-201.
31. Sahiner B, Chan HP, Roubidoux MA, Helvie MA, Hadjiiski LM, Ramachandran A, Paramagul C, LeCarpentire GL, Nees A, and Blane C. Computerized characterization of breast masses on three-dimensional ultrasound volumes. *Medical Physics 31*, 4(2004), 744-754.
32. Boukerroui D, Baskurt A, Boble JA, and Basset O. Segmentation of ultrasound images - multiresolution 2D and 3D algorithm based on global and local statistics. *Pattern Recognition Letters 24*, 4-5(2003), 779-790.
33. Xiao G, Brady M, Noble JA, and Zhang Y. Segmentation of ultrasound B-mode images with intensity inhomogeneity correction. *IEEE Trans. on Medical Imaging 21*, 1(2002), 48-57.
34. Cheng HD, Hu LM, Tian JW, and Sun L. A novel Markov random field segmentation algorithm and its application to breast ultrasound image analysis. In *6th International Conference on Computer Vision, Pattern Recognition and Image Processing*, 2005, 644-647.
35. Boukerroui D, Basset O, Guerin N, and Baskurt A. Multiresolution texture based adaptive clustering algorithm for breast lesion segmentation. *European J. Ultrasound 8*, 2(1998), 135-144.
36. Yap MH, Edirisinghe EA, and Bez HE. Fully automatic lesion boundary detection in Ultrasound breast image. *SPIE Medical Imging Conference*, 6512651231, 17th-22nd February, San Dieg, CA, US(2007).
37. Lee M, Chen Y, Kin S, and Kin K. Geometric active model for lesion segmentation on breast ultrasound images. *IEEE 11th International Conference*, 11(2011), 150-157.
38. Kotropoulos C, and Pitas I. Segmentation of ultrasonic images using support vector machines. *Pattern Recognition Letters 24*, 4-5(2003), 715-727.
39. Zhan Y, and Shen D. Deformable segmentation of 3-D prostrate images using statistical texture matching algorithm. *IEEE Trans. on Medical Imaging 25*, 3(2006), 256-272.
40. Wu HM, and Lu HHS. Iterative sliced inverse regression for segmentation of ultrasound and MR images. *Pattern Recognition 40*, 12(2007), 3492-3502.
41. Dokur Z, and Olmez T. Segmentation of ultrasound images by using a hybrid neural network. *Pattern Recognition Letters 23*, 14(2002), 1825-1836.
42. Iscan Z, Kurnaz MN, Dokur Z, and Olmez T. Letter: Ultrasound image segmentation by using wavelet transform and self-organizing neural network. *Neural Information Processing – Letters and Reviews 10*, 8-9(2006).
43. Huang YL, and Chen DR. Watershed segmentation for breast tumor in 2-D sonography. *Ultrasound in Medicine & Biology 30*, 5(2004), 625-632.
44. Gomez W, Lejia L, Alvarenga AV, Infantosi AFC, and Pereira WCA. Computerized lesion segmentation of breast ultrasound based on marker-controlled watershed transformation. *Medical Physics 37*, 1(2010), 82-95.
45. Huang CS, Wu CY, Chu JS, Lin JH, Hsu SM, and Chang KJ. Microcalcifications of non-palpable breast lesions detected by ultrasonography: correlation with mammography and hispathology. *Ultrasound in Obstetrics and Gynecology 13*, 6(1999), 431-436.
46. Chen CM, Chou YH, Chen CSK, Cheng JZ, Ou YF, Yeh FC, and Chen KW. Cell competition algorithm: A new segmentation algorithm for multiple objects with irregular boundaries in ultrasound images. *Ultrasound in Medicine & Biology 31*, 12(2005), 1647-1664.
47. Cheng JZ, Chou YH, huang CS, Chang YC, Tiu CM, Yeh FC, Chen KW, Tsou CH, and Chen CM. ACCOMP: Augmented cell competition algorithm for breast lesion demarcation in sonography. *Medical Physics 37*, 12(2010), 6240-6252.
48. Cheng JZ, Chen CM, Chou YH, Chen CSK, Tiu CM, and Chen KW. Cell-based two-region competition algorithm with a map framework for boundary delineation of a series of 2D ultrasouind images. *Ultrasound in Medicine & Biology 33*, 10(2007), 1640-1650.
49. L Zhang, Y Ren, C Huang, F Liu. "A novel automatic tumor detection for breast cancer ultrasound images". *Eighth International Conference on Fuzzy Systems and Knowledge Discovery (FSKD)*, vol.4, pp.401-404, July 2011.
50. Cheng HD, and Chen JR. "Automatically determine the membership function based on the maximum entropy principle". *Information Sciences* vol. 97, pp. 163-182, February 1997.
51. Chan TF, and Vese LA. "Active contours without edges", *IEEE Trans. On Image Processing*, vol.10, pp.266-277, February 2001.
52. M Kass, A Witkin, D Terzopoulos. Snakes: active contour models. *International Journal of Computer Vision* 1(1998) 321-331.
53. N Xu, N Ahuja, R Bansal. Object segmentation using graph cuts based active contours. *Computer Vision and Image Understanding* 107(2007) 210-224.
54. V Caselles, R Kimmel, G Sapiro. Geodesic active contours. In *Proceedings of IEEE Internationcal Conference on Computer Vision*'95, Boston, MA, 1995, pp.694-699.
55. GP Zhu, SQ Zhang, QS Zeng, CH Wang. Boundary-based image segmentation using the binary level set method. *Optical Engineering* 46(2007) 050501.
56. K Zhang, L Zhang, H Song, and W Zhou. "Active contours with selective local or global segmentation: A new formulation and level set method". *Image and Vision Computing*, vol.28, no.4, pp.668-676, 2010.
57. D Mumford, J Shah. Optimal approximation by piecewise smooth function and associated variational problems. *Communitcation on Pure and Applied Mathematics* 42(1989) 577-685.
58. C Li, C Kao, JC Gore, Z Ding. Minimization of region-scalable fitting energy for image segmentation. *IEEE Trans. On Image Processing* 17(2008) 1940-1949.
59. P Perona, J Malik. Scale-space and edge detection using anisotropic diffusion. *IEEE Trans. on Pattern Analysis and Machine Intelligence* 12(1990) 629-640.
60. Moon WK, Huang CS, Shen WC. Analysis of elastographic and B-mode features at sonoelastography for breast tumor classifcation. *Ultrasound Med Biol*, 2009 Nov; 35(11):1794-802.

61. Chang R, Shen W, Yang M. Computer-aided diagnosis of breast color elastography. In: *Proceedings of the International Society for Optical Engineering*, Bellingham, WA; 2008:69150I.1-69150I.9.